Effect of Chemistry and Morphology on the Biofunctionality of Self-Assembling Diblock Copolypeptide Hydrogels

Lisa M. Pakstis,† Bulent Ozbas,† Kelly D. Hales,† Andrew P. Nowak,‡ Timothy J. Deming,‡ and Darrin Pochan*,†

Departments of Materials Science and Engineering and Delaware Biotechnology Institute, University of Delaware, Newark, Delaware 19716, and Departments of Materials and Chemistry and Materials Research Laboratory, University of California, Santa Barbara, Santa Barbara, California 93106

Received July 18, 2003; Revised Manuscript Received September 21, 2003

Amphiphilic, diblock copolypeptides of hydrophilic lysine or glutamic acid and hydrophobic leucine or valine have been observed to self-assemble into rigid hydrogels in aqueous solution at neutral pH and very low volume fraction of polymer, ≥0.5 wt % polypeptide. Laser scanning confocal microscopy and ultra small angle neutron scattering revealed a heterogeneous microstructure with distinct domains of hydrogel matrix and pure water pores. In situ nanoscale characterization, using cryogenic transmission electron microscopy, revealed a porous, interconnected membranous network of assembled polypeptides. At concentrations of polypeptide below gelation, diblocks containing lysine were cytotoxic to cells, whereas those containing glutamic acid were noncytotoxic. At higher polypeptide concentrations, within rigid gel scaffolds, both lysine and glutamic acid based diblocks were noncytotoxic but did not support cell attachment/proliferation. The cationic chemistry observed as cytotoxic in the fluid state was essentially inert in the intact, rigid hydrogel state.

Hydrogels are being explored as potential tissue engineering scaffolds because of their hydrophilicity, diversity of chemical modification, and possible biocompatibility.[1] Much effort has been devoted to processing microscale porosity into materials for potential tissue engineering scaffolds. High degrees of porosity in the microstructure increase the surface area of the material and, thus, promote increased cellular attachment. In addition, interconnecting pores on the nano- up to microscale within the scaffold ensure cellular viability by allowing cell motility and transportation of waste products, nutrients, oxygen, and metabolites.[2] Microscale porosity also helps promote eventual tissue/organ viability by supporting the possible formation of a vascular network. Additionally, hydrogels are attractive tissue engineering scaffolds because they may mimic the extracellular matrix by controlling tissue structure and regulating cellular function.[3] The specific ability to design in and control the structure of a hydrogel would allow one to affect or control many or all of the properties critical to the success of a tissue engineering scaffold. We have discovered a self-assembled hydrogel system with an innate, heterogeneous microscale morphology that allows us to specifically observe structure/bioproperty relationships and probe the feasibility of these peptide-based materials as potential biomaterials.

Currently, tissue engineering scaffolds are formed by the addition of a cross-linking agent to a synthetic biocompatible polymer, such as poly(vinyl alcohol), PVA,[4] poly(D,L-lactic-*co*-glycolic acid), PLGA,[5] and poly(2-hydroxyethyl methacrylate), PHEMA,[6] or to a naturally occurring polymer such as gelatin[7] or alginate.[8] These hydrogels are innately homogeneous on the microscale and require additional processing techniques, including freeze−thaw,[9] particulate leaching,[10,11] microsphere sintering,[12] or nonwoven fiber formation,[13] to make them suitable for tissue engineering applications. Attempts have been made to circumvent pore fabrication through direct photoencapsulation[14] of cells within a hydrogel matrix to produce a scaffold with uniform cell density. In all cases, the scaffold must be designed to ensure cellular mobility and nutrient transport throughout the material. Materials for various biological applications have also been formed through the self-assembly of biomolecules and bioconjugates in systems where a peptide headgroup is attached to a dialkyl tail to form tubules[15] or gels[16] for biomineralization as well as low molecular weight β-sheet forming oligopeptides that self-assemble into fibrillar hydrogels.[17,18]

We are investigating a system of diblock copolypeptides that were found to self-assemble into porous hydrogels at low volume fractions of polypeptide (<1.0 wt %).[19,20] Importantly, the assembled hydrogels inherently contain porosity on both the nano- and microscale. Specifically, the hydrogel morphology consists of pores of pure water on the microscale with a dilute, interconnected membranous network on the nanoscale. The polypeptides studied herein are approximately 200 amino acids in length, consisting of 80 to 90 mol % hydrophilic block of poly(L-lysine) or poly(L-glutamic acid) and 20 to 10 mol % hydrophobic block of poly(L-leucine) or poly(L-valine). In addition to the innately porous morphology, these materials have the advantageous

* To whom correspondence should be addressed. E-mail: pochan@udel.edu.
† University of Delaware.
‡ University of California, Santa Barbara.

10.1021/bm034249v CCC: $27.50
Published on Web 12/30/2003

rheological property of thinning while under shear for ease of processing but are then able to immediately reform via self-assembly after the cessation of shear.[19] The completely peptidic nature of the molecular blocks also provides an opportunity for facile incorporation of specific secondary structure in the blocks in order to manipulate final material properties (e.g. hydrophobe conformation to manipulate gelation concentration[19]). The hierarchical nature and peptide foundation of the scaffold structure provides a nice exploratory platform for tissue engineering applications.

In this study we show that the diblock copolypeptide hydrogel microscale morphology provides hydrogel structures previously obtained only through additional material processing, making these peptidic materials potential candidates for biomedical applications. Importantly, in vitro mammalian culturing experiments show the intact gels to be noncytotoxic despite toxicity of some of the gel-forming molecules in solution at concentrations well below the gelation threshold. These studies demonstrate a morphological dependence on biocompatibility in gels that are self-assembled and may provide a convenient paradigm for new biotechnological hydrogel design.

Experimental Section

Polypeptide Synthesis. All block copolypeptides were synthesized using $Co(PMe_3)_4Co$ initiator,[21] according to literature procedures.[22] Molecular weights of the protected polymers were determined using size exclusion chromatography in *N*,*N*′-dimethylformamide (DMF) using a Wyatt DAWN DSP light scattering detector and Wyatt Optilab DSP. Separations were effected by 10^5, 10^4, and 10^3 Å Phenomenex 5μ columns using 0.1M LiBr in DMF eluent at 60 °C. The protecting groups of N_ϵ-benzyloxycarbonyl-L-lysine residues were removed to give L-lysine·HBr residues in copolypeptides by addition of 33 wt % HBr in acetic acid to a solution of copolymer in trifluoroacetic acid at 0 °C for 1 h. Poly(γ-benzyl-L-glutamate)-containing diblocks were deprotected using trimethylsilyliodide in CH_2Cl_2 at 40 °C for 24 h. All deprotected copolymers were dissolved in deionized water and dialyzed exhaustively against distilled water. Lyophilization of these solutions gave the copolymers as powders, whose structures and compositions were confirmed using ^{1}H and ^{13}C NMR, circular dichroism, and IR spectroscopy.[22] Isolated yields of the deprotected copolymers ranged between 75% and 90%. Amino acid compositions of the copolymers were found to be within 3% of predicted values. Chain lengths of the copolymers were found to be within 8% of predicted lengths with PDI (weight average mass/number average mass) ranging between 1.1 and 1.3. ^{1}H NMR in D_2O indicated a 97−98% removal of benzyloxycarbonyl groups from lysine residues.

Hydrogel Preparation. Freeze-dried polypeptide was dissolved/self-assembled in either deionized water or cell culturing media at neutral pH and room temperature and stood for 12 h before use to ensure complete dissolution. Vortexing the polypeptide solution increased its rate of dissolution but did not alter the final hydrogel structure. For all studies involving fluorescent dyes, the dye solution was added to the desired solvent mixture before addition of the freeze-dried polypeptide (see below).

Laser Scanning Confocal Microscopy (LSCM). Nanomolar concentrations of a lipophilic fluorescent dye (DiO C_{18}, Molecular Probes) in THF were added to the solvent mixtures before polypeptide dissolution to allow for uniform labeling of the hydrogel matrix during self-assembly. The hydrogels were imaged using a Zeiss LSM 510 NLO Microscope with an ArKr laser (30mW) at an excitation wavelength of 488 nm. Additional experiments involved incorporation of both a hydrophilic fluorescent dye (Fluorescein, Molecular Probes) with an amine specific dye (Alexa Fluor 546, carboxylic acid, succinimidyl ester, Molecular Probes) to the solution before polypeptide dissolution for dual dye imaging that highlighted both the water and the hydrogel matrix. Excitation of the hydrophilic dye occurred at 543 nm using a HeNe laser. LSCM, unlike fluorescence microscopy, enables imaging of various *xy* planes within the sample in which the optical slice for all experiments is $<1\mu$m. Information regarding the 3-dimensional hydrogel morphology was obtained by collecting and compiling multiple 2-dimensional slices along the *z* axis. The average depth studied was 50 μm (50 $x-y$ images with a 1 μm optical slice).

Cryogenic Transmission Electron Microscopy (Cryo-TEM). A thin film (∼100 nm in thickness) of assembled hydrogel was transferred to a carbon coated grid and vitrified in liquid ethane at −170 °C using a Leica EM CryoPreparation System. In situ gel morphology was imaged in bright field mode at 200 kV utilizing a Gatan 626 cryoholder and cryotransfer stage in a JEOL 2000FX microscope. Images were captured using Kodak electron film. During observation, the sample holder was kept at −170 °C to inhibit sublimation of vitreous water.

Ultra Small Angle Neutron Scattering (USANS). USANS experiments were performed on the perfect crystal diffractometer (PCD) on beam port BT-5 at the National Center for Neutron Research, National Institute of Standards and Technology, Gaithersburg, MD. Gel samples were formed in vials and transferred to titanium sample cells with 30 mm diameter quartz windows and a 1 mm path length. Care was taken to not introduce any air bubbles into the hydrogel sample. USANS data was collected for 12 h over a q range of $10^{-5}-10^{-3}$ Å^{-1}. Hydrogels for USANS were prepared in D_2O for adequate contrast between the hydrogen-rich gel scaffold matrix and the deuterated solvent. The USANS, Bonse Hart-type diffractometer, produces high q resolution in one direction by using multiple reflections from silicon perfect crystals. A graphite premonochromator is used to select a 2.38 Å neutron wavelength beam. The beam is then diffracted by a three-bounce silicon (220) channel-cut monochromator. After passing through the sample, another three-bounce channel-cut silicon crystal analyzer selects scattering at small angles (θ) in one direction. The data are slit-desmeared as described by Singh et al.[23]

Cell Studies. To assess the chemical cytotoxicity of the polypeptides, low concentrations of polypeptide were dissolved directly in the mammalian cell culture media (DMEM with 10% calf bovine serum, 200mM L-glutamine, and 4.5

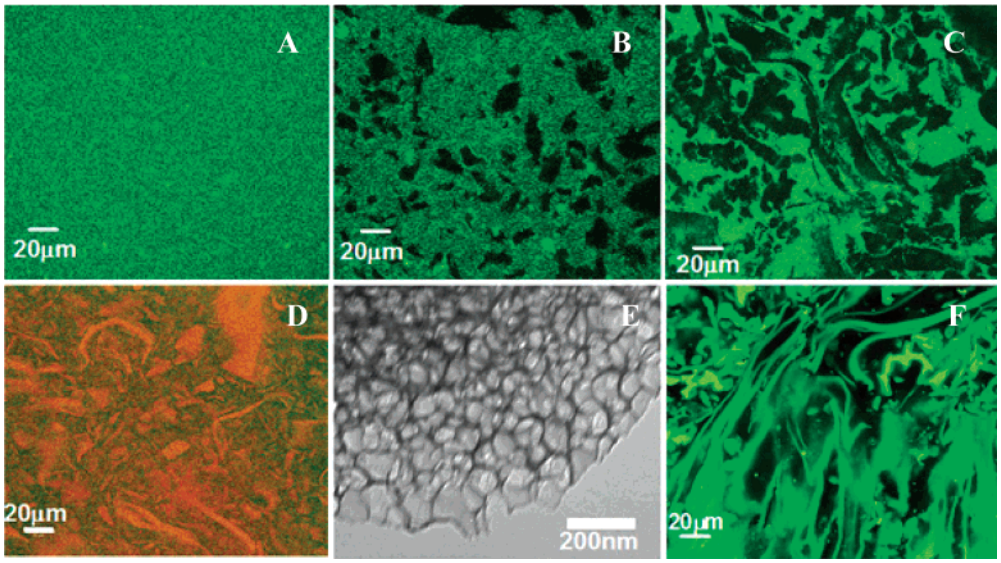

Figure 1. LSCM images of $K_{160}V_{40}$ at concentrations of (a) 0.1, (b) 0.375, and (c) 1 wt % diblock polypeptide showing the highlight of the hydrogel matrix using a lipophilic fluorescent dye, DiO. (d) 1.0 wt % $K_{160}V_{40}$ with the hydrophilic dye fluorescein and an amine specific dye to highlight the regions of pure water (green) and self-assembled polypeptide matrix (red) within the hydrogel. (e) CryoTEM of $K_{160}V_{40}$ at 1 wt % provided in situ imaging of the hydrogel matrix. (f) LSCM of $K_{160}V_{40}$ at 3 wt % in DMEM.

g/L glucose). Mouse fibroblasts (NIH 3T3, ATCC) were added to each sample (polypeptide concentrations: 0.002, 0.0033, 0.0067, and 0.0167 wt %) at an initial density of 1.3×10^4 cells/well and were grown at 37 °C in an environment of 5% CO_2 and 98% humidity. Once the suspended 3T3 cells were added to assay plates containing polypeptide solutions, the cellular viability was measured after 48 h using the MTT Assay.[24,25] Briefly, water-soluble 3-(4,5-dimethylthiazol-2-yl)-2,5-diphenyltetrazolium bromide was added to the cells. Metabolically active cells convert the tetrazolium salt into an insoluble purple formazan salt by reductive cleavage of the tetrazolium ring. After 4 h, a detergent solution was added to solubilize the formazan. The absorbance of the resulting solution was measured at $\lambda = 570$ nm with a reference at $\lambda = 650$ nm using a Beckman Coulter DU 7400 Spectrophotometer. The absorbance intensity at 570 nm is a direct measure of the number of viable cells. Experiments were performed in triplicate.

Additionally, dilute solutions of polypeptides were added to sample wells with adhered NIH 3T3 cells. This was done to both (a) confirm that cell death was the result of polypeptide toxicity rather than polypeptide adhesion to the assay plate preventing cellular attachment and (b) to determine the rate and concentration dependence of the cell death on cultures of viable cells. Cells were seeded at a density of 1.65×10^4 cells/well and incubated at 37 °C, 5% CO_2 and 98% humidity for 24 h to ensure cellular attachment and viability. Dilute solutions of polypeptide were added to the sample well at concentrations of 0.003 wt %, 0.007 wt %, 0.013 wt %, and 0.033 wt %, concentrations well below the gelation threshold. Cell viability was measured using the MTT assay at 2, 6, and 20 h and plotted as time vs % viability for each polypeptide where % viability is the ratio of the absorbance of the polypeptide sample to the control sample.

Cytocompatibility studies of rigid hydrogels were performed by seeding cells on preformed gels. Confluent cells were treated with Cell Tracker Green (Molecular Probes) fluorescent dye in order to monitor the cells within the gel matrix. Hydrogels were prepared by dissolving lyophilized polypeptide in water and swelling with multiple aliquots of DMEM until the final polypeptide concentration was 3.0 wt %. Cells were then added to the bulk and surface of the hydrogels and imaged at 4 and 12 h.

Results and Discussion

Morphology Studies. The microstructure of the self-assembled hydrogel materials has been characterized using LSCM. Figure 1a−c shows the morphology of $K_{160}V_{40}$, an 80 mol % positively charged polyelectrolyte block with a 20 mol % β-strand hydrophobic tail (the secondary structure of the hydrophobe has been previously determined[19] using circular dichroism). The concentrations shown have been rheologically determined to represent the polypeptides (a) in a liquid phase, (b) at the transition of a liquid to a solid, and (c) in the solid, gel phase.[19] The diblock copolypeptides self-assemble in aqueous solution due to hydrophobic interactions between the valine blocks. The consequent hydrophobic cores of the self-assembled gel scaffold can be used to directly image the in situ gel matrix microscale morphology. These hydrophobic domains within the matrix of the hydrogel are accentuated by a lipophilic fluorescent dye and appear green in the images. As the concentration of polypeptide increases, the microscale morphology of the materials changes from a relatively homogeneous liquid to a heterogeneous gel. Channels and pores of water, the black areas in the images, become more defined at higher polypeptide concentrations. All hydrogels are stable, maintaining their innate microscale morphology for months.

Addition of a hydrophilic dye to a 1.0 wt % $K_{160}V_{40}$ sample, shown in Figure 1d, allowed simultaneous imaging of both peptidic and pure water domains within the hydrogel. The hydrogel matrix is highlighted by the amine specific dye that fluoresces red when bound to the lysine residues in the polypeptides. The water within the hydrogel matrix

fluoresces green due to the incorporation of the hydrophilic fluorescein probe. Importantly, green fluorescence is present throughout the gel matrix and in the water-filled pores and channels, confirming a substantial amount of water *within* the gel matrix. In other words, because the concentration of polypeptide required for gelation is so low, the gel scaffold incorporates a large volume fraction of water on the nanoscale.

The dilute nature of the hydrogel matrix was confirmed by cryoTEM. Vitrifying the hydrogel to cryogenic temperatures locked in the nanoscale, self-assembled morphology. By preventing crystallization of the water, this technique provides for the in situ characterization of the hydrogel network. The light gray regions in Figure 1e are the vitrified water, and the dark regions are the scaffold structures formed by the self-assembled polypeptides. On the nanoscale, the self-assembled morphology of $K_{160}V_{40}$ is a highly porous, membranous network surrounded by significant amounts of water. The results of direct nanoscale morphology characterization explain why one observes hydrophilic dye fluorescence in the gel matrix regions on the microscale (Figure 1d) and explain why rigid hydrogel materials are obtained with such a small volume fraction of solid materials.

As shown with cryoTEM in Figure 1e, the edge of the hydrogel contains many open struts and fragments and provides insight into the assembly process for these polypeptides. The polypeptides associate throughout the sample until there is no free peptide in solution, evidenced by the open ends in Figure 1e. With higher concentrations of polypeptide ($\geq$ 0.5 wt %), the polypeptides assemble into an interconnected network, producing a rigid hydrogel with a defined heterogeneous microstructure of water pockets and gel matrix (Figure 1c). At lower concentrations of polypeptide, the chains associate to form self-assembled aggregates that retain liquid properties and appear homogeneous (Figure 1a) on the microscale.

A more quantitative characterization of the microstructure observed in $K_{160}V_{40}$ gels is shown in Figure 2. USANS results from gels with higher polypeptide content, 4.0 and 2.0 wt % respectively, clearly exhibit an approximate -4 scaling of log(I) vs log(q). This limiting slope is indicative of scattering from a surface fractal interface between two phases and has been observed on the microscale in gel systems.[26,27] In this case, the two phases are the gel scaffold matrix, highlighted by green fluorescence in the LSCM from Figures 1a−c, and the water pores and channels, exhibiting no fluorescence and appearing black in these hydrophobic dye images. Therefore, when in the solid gel state, a well-defined boundary exists between the gel matrix regions and the water regions. When the concentration of polypeptide drops to 0.5 wt %, very close to the gel:liquid crossover concentration of ~0.4 wt % as determined rheologically,[19] the slope drops significantly. This drop indicates the presence of a much more ill-defined interface between the gel scaffold matrix and the water channels and pores. This loss of definition between the gel matrix and water pores/channels observed via neutron scattering parallels the real-space microscopy results in Figure 1 where well-defined water domains (Figure 1c) are not observed in the more dilute gels (Figure 1, parts a and b).

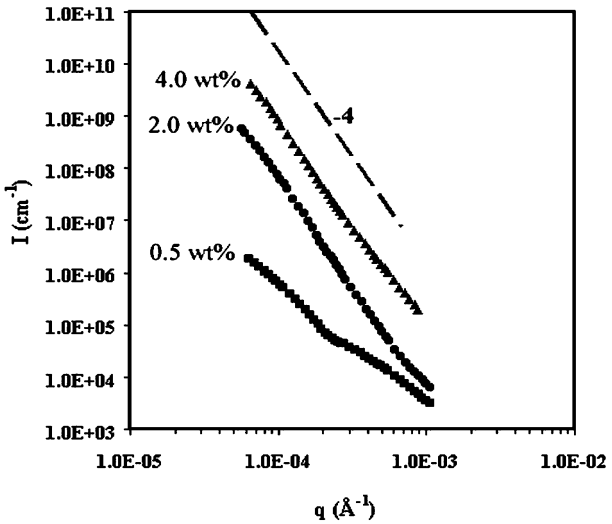

Figure 2. Ultra-small angle neutron scattering from $K_{160}V_{40}$ in D_2O at 4.0 (▲), 2.0 (●), and 0.5 wt % (■) block polypeptide. The 4.0 wt % scattering data is offset by a decade in absolute intensity from the 2.0 wt % data for clarity. Absolute intensity, I, in cm^{-1} is plotted vs the scattering angle, $q = (4\pi/\lambda)\sin(\theta/2)$ where θ is the scattering angle and λ is the neutron wavelength. A -4 slope in log(I) vs log(q) is drawn for comparison with the data. The 4.0 and 2.0 wt % data closely follow the Porod-like -4 scaling, whereas the 0.5 wt % slope drops significantly indicating an ill-defined interface between the gel matrix and the D_2O pores/channels.

When using block copolypeptides to build materials via self-assembly, several molecular parameters, such as relative block lengths, can be manipulated in attempts to affect the final properties of the material. Importantly, by varying amino acid monomers, one can also directly control block secondary structure and charge character. The effect of all of these parameters on the hydrogelation and consequent microscale morphology were observed via LSCM. First, the effect of the hydrophobic block secondary structure on the self-assembled hydrogel morphology was studied using $K_{160}L_{40}$. In these diblock copolypeptides, the hydrophobic tail has been changed from the β-sheet structure of poly(L-valine) to an α helix using poly(L-leucine).[19] The same microstructure is present in $K_{160}L_{40}$ hydrogel down to below 0.50 wt % block polypeptide and is shown at 3.0 wt % in Figure 3a. Despite the morphological similarities between the hydrogels, changing the secondary structure of the hydrophobe did slightly affect the ultimate strength, or percent of block copolypeptide required for solidlike ($G' > G''$) rheological properties, of the hydrogel.[19] For example, gelation of $K_{160}L_{40}$ occurred at 0.25 wt % (hydrogel strength determined rheologically as $G' = 3$ Pa) polypeptide compared to $K_{160}V_{40}$ gelation at 0.375 wt % ($G' = 2$ Pa) polypeptide ($G' = 300$ Pa for both $K_{160}V_{40}$ and $K_{160}L_{40}$ at 1 wt %).[19] Therefore, by changing the secondary structure of the hydrophobic block, one can alter the strength of the hydrogel and retain the innate heterogeneous microstructure.

Large differences in gel moduli at a constant block copolypeptide concentration are also seen when comparing relative hydrophilic to hydrophobic block lengths with gel storage moduli being directly proportional to hydrophobe content.[19] However, the innate heterogeneous microstructure is observed when the length of the hydrophobe is decreased from 20 to 15 mol %, as in the case of $K_{170}L_{30}$, shown at 3.0 wt % in Figure 3b. The innate microstructure due to the

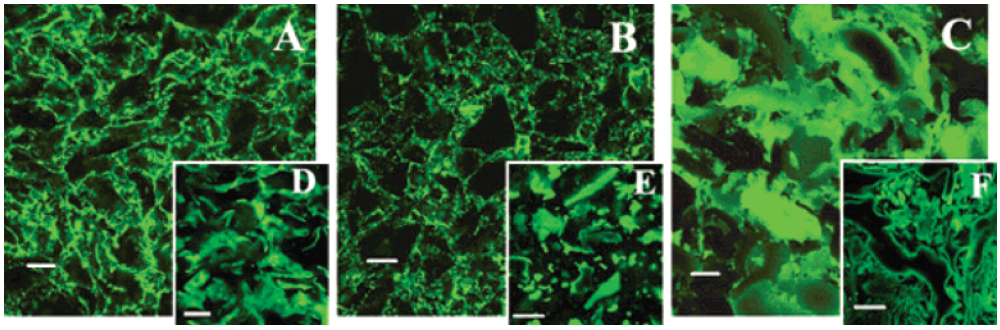

Figure 3. Ubiquitous microstructure of the self-assembled hydrogels shown for polypeptides having (a) a leucine hydrophobic block, $K_{160}L_{40}$, (b) a 15 mol % hydrophobic block, $K_{170}L_{30}$, and (c) an anionic hydrophilic block, $E_{160}L_{40}$, at 3 wt %. Assembly of the polypeptides under physiological conditions in DMEM retains their heterogeneous microstructure as shown at 3 wt % for (d) $K_{160}L_{40}$, (e) $K_{170}L_{30}$, and (f) $E_{160}L_{40}$. All scale bars are 20 μm.

self-assembly of block copolypeptides is also observed when the charge character of the hydrophilic block is changed from cationic L-lysine (K) to anionic L-glutamic acid (E). The morphologies observed for E-based amphiphiles are shown for $E_{160}L_{40}$ at 3.0 wt % in Figure 3c and are similar to that observed for the K-based gels shown in Figures 1 and 3a,b.

To explore the feasibility of using hydrogels constructed via block copolypeptide self-assembly as legitimate tissue engineering scaffolds, one needs to study the gelation behavior and consequent microstructure in buffers and other ionic media. Gelation in the presence of 100 mM NaCl was studied to assess hydrogel properties when the electrostatic interactions of the hydrophilic polyelectrolyte blocks are partially screened. The matrix is slightly more diffuse than in the case of pure water, but the overall porous/channel-filled microstructure remains intact in gels formed from polypeptides with ≥15 mol % hydrophobic block. An extensive study on the behavior of these hydrogels in salts and buffers is currently in progress.

The hydrogels also maintain their microscale heterogeneity under physiological conditions. Gelation of $K_{160}L_{40}$ at 3.0 wt %, Figure 3d, in the presence of cell culturing media (DMEM) reveals a more diffuse matrix than that in pure water; however, the microscale heterogeneity is maintained. When decreasing the hydrophobic block to 15 mol % with $K_{170}L_{30}$, the hydrogel matrix is somewhat disrupted, Figure 3e. Further decreasing the hydrophobic block to 10 mol % with $K_{180}L_{20}$ (not shown), changing the hydrophilic block to anionic glutamic acid with $E_{160}L_{40}$, Figure 3f, or changing the hydrophobic block to valine with $K_{160}V_{40}$, Figure 1f, increases the heterogeneity of the hydrogel microstructure in DMEM.

Cell Studies. In constructing rigid hydrogels via very dilute diblock copolypeptide self-assembly, one can be flexible in choosing a relative block length (altering the fraction of the hydrophobic block from 10 to 20 mol %), charge character of the hydrophilic block (cationic L-lysine vs anionic L-glutamic acid), and a secondary structure of the hydrophobic block (α helix and β sheet) in order to tailor specific hydrogel properties. Importantly, a heterogeneous microstructure (and dilute nanostructure) was observed for all of these assembling molecules; giving material properties that are critical for viable tissue engineering scaffolds. Another fundamental property of a potential scaffold for tissue engineering is how it interacts with implanted cells that will be cultured into a viable tissue. At the simplest level,

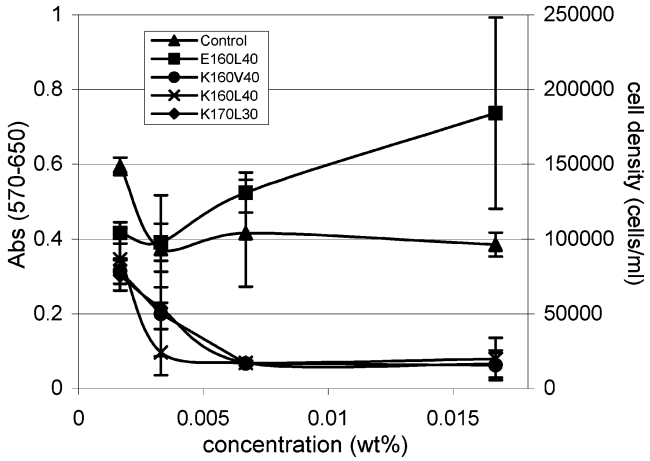

Figure 4. Cytotoxicity studies with fibroblasts showing that glutamic acid polypeptides are not cytotoxic and induce slightly increased viability of the cells. All lysine-based polypeptides are cytotoxic at concentrations greater than 0.0050 wt % polypeptide.

the scaffold must not be cytotoxic. The biocompatibility of these block copolypeptides was assessed with mammalian cell studies. Quantitative measurements of the cytotoxicity of block copolypeptides were performed with assays that involved the use of low concentrations of block copolypeptides below the gelation concentrations such that the molecules were dispersed in a free-flowing solution, probably as micelles.[28] These studies with dilute polymer were a purely chemical assay of the samples and were performed to determine the cytotoxic effects resulting from the functionality of the polypeptides. Subsequent studies involved cell culturing on rigid, assembled hydrogels in cell culturing medium as the substrate. Thus, a direct comparison could be made between the cytotoxicity of the block copolypeptides in solution and when trapped within an intact, rigid hydrogel. In other words, a direct observation of the hydrogel morphological effects on block copolypeptide cytotoxicity could be assessed.

Figure 4 shows the cytotoxicity of the polypeptides to suspensions of mouse fibroblasts, NIH 3T3. Polypeptides containing L-glutamic acid at low concentrations, below 0.0070 wt %, behaved similarly to the control. However, with increasing concentrations of polypeptide, 3T3 cells showed slightly increased growth over the control. Cationic polypeptides containing a poly(L-lysine) block were slightly cytotoxic at concentrations less than 0.0040 wt %, showing approximately 50% viability as compared to the control. At

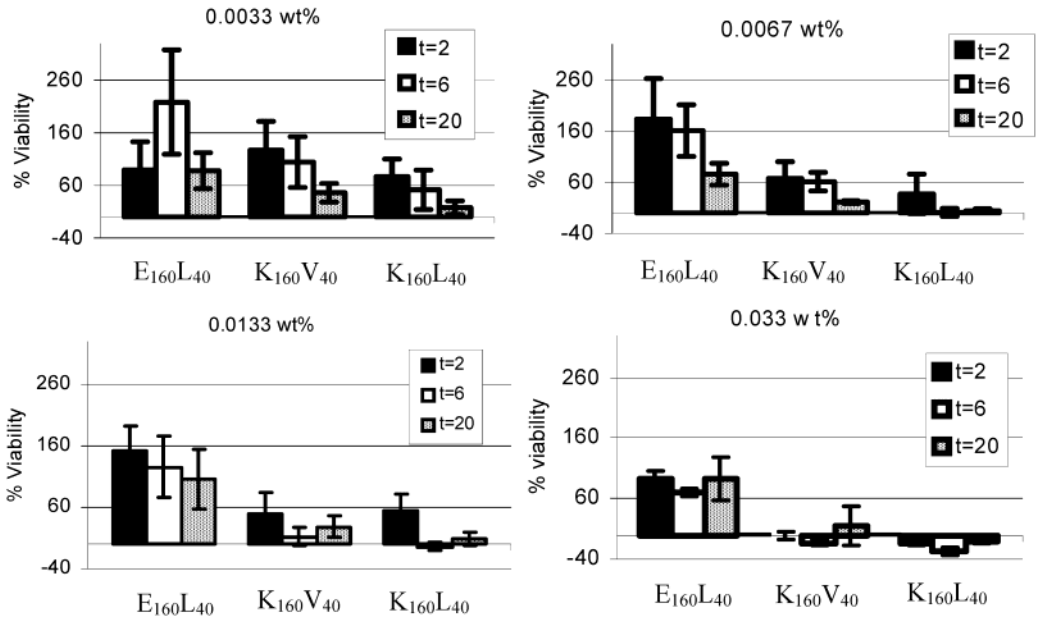

Figure 5. Rate and concentration dependence of cytotoxicity determined using NIH 3T3 cells. Glutamic acid polypeptides experience no cytotoxicity and, in most cases, increased growth as compared to the control at all concentration regimes. At low concentrations of polypeptide, lysine polypeptides do not cause significant cell death immediately, with cell death occurring at approximately 20 h. Higher concentrations of lysine polypeptides induce cytotoxicity within 6 h.

concentrations above 0.0040 wt %, polypeptides containing lysine blocks were completely cytotoxic. Identical cytotoxic behavior of these polypeptides has also been seen using human embryonic kidney (HEK293) cells. Although not shown, cationic polypeptides are completely cytotoxic below 0.004 wt %, and anionic polypeptides are noncytotoxic to concentrations greater than 0.05 wt %.

These studies support previous findings that highly positively charged polypeptides are cytotoxic to various types of mammalian cells.[29−31] Flexible, linear polycations, like the lysine containing copolymers, are thought to be cytotoxic to cells due to the electrostatic interaction between the cationic polypeptides and the anionic phospholipids[29,30] in the cell membranes. The cationic polypeptide possibly undergoes a conformational change disrupting the cell membrane and causing cell death. Anionic molecules, such as the polypeptides containing a glutamic acid block described here, do not have an affinity for the cell membrane and are less problematic.

To ensure that cytotoxicity is the result of polypeptide interactions with cells rather than polypeptide adhesion to the assay plate preventing cellular attachment, experiments were performed in which dilute solutions of polypeptide were added to subconfluent monolayers of cells. These experiments also enabled determination of the rate and concentration dependence of cytotoxicity of these dilute polypeptide solutions. Studies were performed using a concentration range of 0.003 to 0.033 wt % diblock polypeptide at 2, 6, and 20 h after addition, shown in Figure 5. Glutamic acid polypeptides remained biocompatible with ≥90% cellular viability as compared to the control in all cases except for 0.0067 wt % after 20 h that exhibited ≥75% cellular viability as compared to the control. All polypeptides containing lysine blocks, $K_{160}L_{40}$ and $K_{160}V_{40}$, however, behaved similarly and induced cytotoxicity. At low concentrations of polypeptide, 0.003 to 0.007 wt %, the fibroblasts did not experience significant cytotoxic effects until 20 h after incubation with the polypeptides. By increasing the concentration to 0.013 wt %, the cells maintained 50−70% viability, as compared to the control, within 2 h of incubation. Extreme cytotoxic effects were seen within 6 h of incubation with the lysine block polypeptides, inducing approximately 90% cytotoxicity. The rate of cytotoxicity was dramatically increased with higher concentrations of lysine containing block copolypeptides. Cells experienced 90% cytotoxicity within 2 h of incubation with 0.033 wt % polypeptide.

These cellular assays have shown that the cationic polypeptides studied here are cytotoxic at extremely low concentrations of polypeptide, when not in the hydrogel state, whereas anionic polypeptides are cytocompatible. Therefore, cytotoxicity is caused by the chemistry of the hydrophilic blocks of the polypeptides. Based on these results, anionic glutamic acid polypeptides may be more attractive materials for use as potential tissue engineering scaffolds.

To proceed further, it was important to verify that the cell interactions with polypeptides observed in the dilute fluid state would be identical to the interactions with concentrated gels. Surprisingly, initial morphological studies, using higher concentrations of polypeptide to form solid and rigid gels, showed that both cationic and anionic polypeptides were promising substrates for tissue engineering. Fibroblasts added to 2.0−5.0 wt % hydrogels in DMEM revealed that all gels sustain cell viability for time periods up to 12 h but do not allow for cell attachment or proliferation. The cells, in the presence of the hydrogel matrix, retain their spherical shape, as shown in Figure 6, after 4 and up to 12 h. Therefore, cellular viability relative to the chemistry of the gel scaffold is influenced, to a large degree, by the hydrogel morphology because all of the polypeptide is incorporated into the hydrogel network and not available in solution to cause cytotoxicity. Although cytocompatibility is a vital requirement for a feasible cell growth substrate, the promotion of cell attachment and proliferation is obviously also necessary. Other cytocompatible hydrogel matrices being studied for

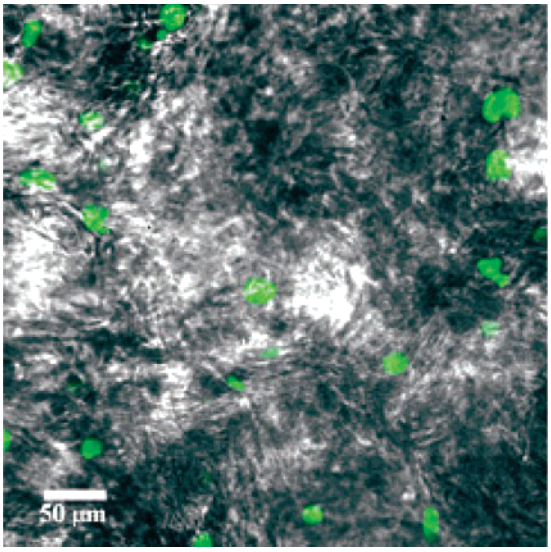

Figure 6. Fibroblasts, labeled with cell tracker green fluorescent dye, seeded within an $E_{160}L_{40}$ hydrogel at 3.0 wt %. The cells remain spherical in shape, indicating that they are viable but not attached, after 4 and up to 12 h.

tissue engineering applications, such as poly(ethylene glycol)-based networks[32] require specific chemoattractants to be chemically added to the network chemistry in order to promote cell adhesion. The design of new block copolypeptides containing additional biofunctionality within the block copolypeptide primary structure, e.g., Arg−Gly−Asp or RGD located at the end of the hydrophilic block,[33,34] is the next step for providing these materials with a complete set of desired biomaterial properties.

Conclusions

The polypeptides described above self-assemble into hydrogels with a porous microstructure at low concentrations of polypeptide and in high ionic strength medium. The heterogeneity of these hydrogels is ubiquitous regardless of the charge of the hydrophilic group or the secondary structure of the hydrophobic group. Because of their innate porosity, which would allow for cell and nutrient mobility, these hydrogels make attractive matrixes for tissue engineering. In addition, this chemically benign gelation strategy may allow for self-assembly and gel formation in the presence of cells for direct, 3-D incorporation of medium and cells throughout the matrix.[35] Initial biocompatibility studies revealed that the anionic polypeptides are noncytotoxic to cells, whereas cationic polypeptides are cytotoxic when used in concentrations well below their gelation concentrations. However, cells remained viable when cultured within both the cationic and anionic hydrogels, indicating that the morphology of the hydrogels prevents cell death. Future work is directed at the covalent incorporation of bioactive sites[34,36] on the copolymers to increase cellular attachment at the hydrogel surface.

Acknowledgment. We acknowledge the support of the National Institute of Standards and Technology, U.S. Department of commerce, in providing the neutron research facilities, supported in part by the National Science Foundation under Agreement No. DMR-9986442, used in this work. LMP and DJP thank John Barker and Man-Ho Kim for help with running USANS experiments and data reduction. This work was partially supported by the MRSEC Program of the National Science Foundation at UCSB under Award No. DMR00-80034, by NSF via award CTS-9986347, and DuPont (DJP and the young faculty award). The authors thank Clifford Robinson (University of DE) for HEK293 cells.

References and Notes

(1) Hoffman, A. S. *Adv. Drug Delivery Rev.* **2002**, *54*, 3−12.
(2) Sieminski, A. L.; Gooch, K. J. *Biomaterials* **2000**, *21*, 2233−2241.
(3) Lee, K. Y.; Mooney, D. J. *Chem. Rev.* **2001**, *101*, 1869−1879.
(4) Peppas, N. A.; Stauffer, S. R. *J. Controlled Release* **1991**, *16*, 305−310.
(5) Ishaug, S. L. C., G. M.; Miller, M. J.; Yasko, A. W.; Yaszemski, M. J.; Mikos, A. G. *J. Biomed. Mater. Res.* **1997**, *36*, 17−28.
(6) Oxley, H. R.; Corkhill, P. H.; Fitton, J. H.; Tighe, B. J. *Biomaterials* **1993**, *14*, 1064−1072.
(7) Tabata, Y.; Hijikata, S.; Ikada, Y. *J. Controlled Release* **1994**, *31*, 189−199.
(8) Shapiro, L.; Cohen, S. *Biomaterials* **1997**, *18*, 583−590.
(9) Hassan, C. M.; Peppas, N. A. *J. Appl. Polym. Sci.* **2000**, *76*, 2075−2079.
(10) Martin, I.; Shastri, V. P.; Padera, R. F.; Yang, J.; Mackay, A. J.; Langer, R.; Vunjak-Novakovic, G.; Freed, L. E. *J. Biomed. Mater. Res.* **2001**, *55*, 229−235.
(11) Mikos, A. G.; Thorsen, A. J.; Czerwonka, L. A.; Bao, Y.; Langer, R.; Winslow, D. N.; Vacanti, J. P. *Polymer* **1994**, *35*, 1068−1077.
(12) Borden, M.; Attawia, M.; Khan, Y.; Laurencin, C. T. *Biomaterials* **2002**, *23*, 551−559.
(13) Mikos, A. G.; Bao, Y.; Cima, L. G.; Ingber, D. E.; Vacanti, J. P.; Langer, R. *J. Biomed. Mater. Res.* **1993**, *27*, 183−189.
(14) Bryant, S. J.; Anseth, K. S. *Biomaterials* **2001**, − *22*, − 626.
(15) Lee, K. C.; Carlson, P. A.; Goldstein, A. S.; Yager, P.; Gelb, M. H. *Langmuir* **1999**, *15*, 5500−5508.
(16) Hartgerink, J. D.; Beniash, E.; Stupp, S. I. *Science* **2001**, *294*, 1684−1688.
(17) Collier, J. H.; Hu, B. H.; Ruberti, J. W.; Zhang, J.; Shum, P.; Thompson, D. H.; Messersmith, P. B. *J. Am. Chem. Soc.* **2001**, *123*, 9463−9464.
(18) Zhang, S. G.; Holmes, T. C.; Dipersio, C. M.; Hynes, R. O.; Su, X.; Rich, A. *Biomaterials* **1995**, *16*, 1385−1393.
(19) Nowak, A. P.; Breedveld, V.; Pakstis, L.; Ozbas, B.; Pine, D. J.; Pochan, D.; Deming, T. J. *Nature* **2002**, *417*, 424−428.
(20) Pochan, D. J.; Pakstis, L.; Ozbas, B.; Nowak, A. P.; Deming, T. J. *Macromolecules* **2002**, *35*, 5358−5360.
(21) Klein, H. F.; Rsch, H. H. *Chem. Ber.-Recueil* **1975**, *108*, 956−966.
(22) Deming, T. J. *Macromolecules* **1999**, *32*, 4500−4502.
(23) Singh, M. A.; Ghosh, S. S.; Shannon, R. F. *J. Appl. Crystallogr.* **1993**, *26*, 787−794.
(24) Slater, T. F.; Sawsyer, B.; Strauchli, U. *Biochim. Biophys. Acta* **1963**, *77*, 383−393.
(25) Mosmann, T. *J. Immunol. Methods* **1983**, *65*, 55−63.
(26) Horkay, F.; Hecht, A. M.; Grillo, I.; Basser, P. J.; Geissler, E. *J. Chem. Phys.* **2002**, *117*, 9103−9106.
(27) Takeshita, H.; Kanaya, T.; Nishida, K.; Kaji, K. *Physica B* **2002**, *311*, 78−83.
(28) Nam, Y. S.; Kang, H. S.; Park, J. Y.; Park, T. G.; Han, S. H.; Chang, I. S. *Biomaterials* **2003**, *24*, 2053−2059.
(29) Morgan, D. M. L.; Clover, J.; Pearson, J. D. *J. Cell Sci.* **1988**, *91*, 231−238.
(30) Morgan, D. M. L.; Larvin, V. L.; Pearson, J. D. *J. Cell Sci.* **1989**, *94*, 553−559.
(31) Choksakulnimitr, S.; Masuda, S.; Tokuda, H.; Takakura, Y.; Hashida, M. *J. Controlled Release* **1995**, *34*, 233−241.
(32) Han, D. K.; Hubbell, J. A. *Macromolecules* **1997**, *30*, 6077−6083.
(33) Rowley, J. A.; Madlambayan, G.; Mooney, D. J. *Biomaterials* **1999**, *20*, 45−53.
(34) Schmedlen, K. H.; Masters, K. S.; West, J. L. *Biomaterials* **2002**, *23*, 4325−4332.
(35) Burdick, J. A.; Anseth, K. S. *Biomaterials* **2002**, *23*, 4315−4323.
(36) Hern, D. L.; Hubbell, J. A. *J. Biomed. Mater. Res.* **1998**, *39*, 266−276.

BM034249V